Available online at www.sciencedirect.com
SCIENCE DIRECT
ELSEVIER
Polymer 46 (2005) 4722–4734
polymer
www.elsevier.com/locate/polymer

Effects of epoxy treatment of organoclay on structure, thermo-mechanical and transport properties of poly(ethylene terephthalate-*co*-ethylene naphthalate)/organoclay nanocomposites

Mingfang Lai, Jang-Kyo Kim*

Department of Mechanical Engineering, Hong Kong University of Science and Technology, Clear Water bay, Kowloon, Hong Kong, China

Received 13 September 2004; received in revised form 3 March 2005; accepted 23 March 2005
Available online 19 April 2005

Abstract

Poly(ethylene terephthalate-*co*-ethylene naphthalate) (PETN) nanocomposites containing two different organoclays, Cloisite 20A and 30B, were prepared by melt intercalation using an extruder. The organoclays was treated with epoxy monomer to further improve the polar interactions with PETN matrix. The morphological, thermal-mechanical, mechanical and gas barrier characteristics of the nanocomposites were evaluated using several characterization tools. It is found that the Cloisite 30B had better interactions with PETN and was more uniformly dispersed within PETN than Cloisite 20A. Epoxy treatment of Cloisite 30B organoclay resulted in improvements in *d*-spacing between silicate layers, thermo-mechanical and tensile properties, as well as thermal stability, processing and gas barrier characteristics of the PETN/30B nanocomposites. These results suggest that the epoxy acted as the compatibilizer as well as the chain extender, improving the chemical interactions between PETN and organoclay, while discouraging the macromolecular mobility of polymer chains in the vicinity clay particles. The implications and the mechanisms behind these observations are discussed.

Keywords: Poly(ethylene terephthalate-*co*-ethylene naphthalate); Organoclay; Nanocomposite

1. Introduction

Polymer layered silicate composites have attracted a great deal of attention both from industry and academia, because these nanocomposites exhibit markedly improved properties when compared with pure polymers or conventional microcomposites. Numerous studies have demonstrated that addition of only a few wt% of layered silicate can lead to wide array of property enhancements of polymers, e.g. increased stiffness and strength [1–4], improved solvent and UV resistance [5,6], enhanced moisture and gas barrier properties [7–10], and superior flame retardancy [11,12].

Several methods have been successfully employed to produce polymer nanocomposites reinforced with organoclays, i.e. intercalation of polymer from solution [13–15], in situ intercalative polymerization and melt intercalation [16–18]. Direct melt intercalation has been recognized as a promising approach in recent years because its great advantages over the other manufacturing methods: this method is environmentally benign due to the absence of organic solvents, and is compatible with many current industrial processes, such as extrusion and injection moulding processes [19,20].

Poly(ethylene terephthalate) (PET), a polymer with low cost, high mechanical performance and chemical resistance, has found a variety of applications such as fibers, bottles, films, and engineering plastics for automobiles and electronics [21]. Nanocomposites, based on PET and nylon, have been utilized as a single-layer container, as the barrier layer in a multi-layer container, or as a coating to the preformed PET film or bottles. A primary objective of the development of PET–clay nanocomposites was to improve the gas barrier property that is required for beverage and food packaging. The morphological, physical, thermal and mechanical properties of the PET–clay nanocomposites have been extensively investigated and well documented [22–32]. The melt-intercalation technique

* Corresponding author. Tel.: +852 2358 7207; fax: +852 2358 1543.
E-mail address: mejkkim@ust.hk (J.-K. Kim).

0032-3861/$ - see front matter © 2005 Elsevier Ltd. All rights reserved.
doi:10.1016/j.polymer.2005.03.062

was used to fabricate the nanocomposites [29–32], and significant improvements in mechanical properties compared to neat PET were reported. However, the low melting viscosity and the narrow processing window frequently experienced during the melt-intercalation of PET made it rather difficult to process, compared to other thermoplastics. A systematic increase in melt viscosity of PET was reported [29,32] with increasing clay concentration, indicating further thermal degradation. PET nanocomposites were prepared by melt compounding PET with organically modified MMT (treated with 1,2-dimethyl-3-*N*-hexadecyl imidazolium, a modifier with high thermal stability) under various blending conditions [31]. The composites showed a high degree of clay dispersion and exfoliation. Alternative mixing conditions, longer residence times and higher screw speeds resulted in poor quality nanocomposites.

This paper forms a larger project on the development of polymer–organoclay nanocomposites that possess much improved moisture/gas barrier characteristics, as well as antimicrobial capabilities for food and beverage packaging materials. In this study, poly(ethylene terephthalate-*co*-ethylene naphthalate) (PETN) nanocomposites containing two different kinds of commercial organoclay were successfully produced based on the melt intercalation technique. An epoxy monomer was added to further improve the polar interactions between the organoclay and the matrix, which in turn enhance the thermal stability of the composites. The morphological, thermal, mechanical and gas barrier properties of the nanocomposites were measured based on several characterization tools.

2. Experimental

2.1. Materials and preparation of nanocomposites

A commercial grade PETN copolymer resin (Noplake831, supplied by Kolon Industries, Korea), composed of 92 mol% of ethylene terephthalate content, was used throughout this work. Two modified montmorillonites (supplied by Southern Clay Products, USA) were studied: Cloisite 20A (MMT-Alk; modified by dimethyl 2-ethylhexyl (hydrogenated tallowalkyl) ammonium cation) and Cloisite 30B (MMT-$(OH)_2$; modified by methyl bis(2-hydroxyethyl) (hydrogenated tallowalkyl) ammonium-cation), which contained 26 and 21 wt% of organics, respectively. The chemical structures of the organo-modifiers are presented in Fig. 1. To further enhance the polar interactions between the organoclay and the PETN matrix, the organoclay surface was treated with a diepoxide, a diglycidyl ether of bisphenol A (DGEBA) (Epon828, supplied by Shell, Hong Kong Ltd.) with epoxy molar mass of 184–190. The epoxy monomer was diluted with acetone in the volume ratio of 1:10. The organoclay was first suspended in water, and then a desired amount of epoxy-acetone solution was purged into the mixture, followed by

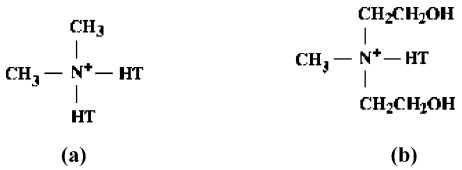

Fig. 1. Chemical structures of organo-modifiers used in (a) Cloisite 20A and (b) 30B clays. HT is hydrogenated tallow (~65% C18; ~30% C16; ~5% C14).

mechanical stirring at 50 °C for 2 h. The mixture was dried completely in an oven to evaporate the water and solvent. The weight ratio of epoxy to PETN (0.75/100) in the finished composite was calculated according to the molecular weight of epoxy and carboxyl content of PETN [33]. The composites were fabricated via melt intercalation. The PETN pellets were dried in a vacuum oven at 80 °C for at least 10 h before use. PETN was mixed with treated organoclay in a twin screw extruder (Collin, Teach-line ZK 25T) at a rotor speed of 50 rpm, the temperature profiles of the barrel were 210–230–250–230 °C from hopper to die.

2.2. Characterization of nanocomposites

The morphological, thermomechanical, rheological, mechanical and gas barrier properties of nanocomposites were characterized using various tools X-ray diffraction (XRD) (Philips PW 1830, Cu K_a radiation: 1.54056 Å) analysis was carried out to measure the *d*-spacing of dry clay powder, premixed clay and the composites at a scanning rate of 0.1°/min from 2 to 10°. A bright field transmission electron microscope (TEM, JEOL 2010) was used to examine the sample cross sections at an acceleration voltage of 120 kV. Ultrathin sections of nanocomposites (ca. 80 nm thick) were prepared using a Leica Ultracut R ultra-cryomicrotome.

Thermomechanical properties of nanocomposites were characterized using a DSC-92 instrument (Setaram). Samples of 10 ± 1 mg were encapsulated in aluminum pans and heated from 25 to 280 °C at a ramp rate of 10 °C/min, followed by holding at 280 °C for 3 min to destroy the crystalline nuclei completely. The cooling traces were recorded from 280 to 50 °C, and then the second heating scan was recorded. The melting temperature was taken from temperature corresponding to the peak value. The thermal stability was evaluated using a thermo-gravitational analyzer (TGA-7 by Perkin–Elmer) by heating samples from room temperature up to 600 °C at a heating rate of 20 °C/min under a nitrogen flow. Time dependence of weight loss of PETN/clay composites was analyzed at 300 °C.

PETN plates of 1 mm in thickness were prepared by compression moulding at 260 °C. The mould was quenched using cold water, followed by annealing at 150 °C for 2 h. The plates were cut into size 20×4 mm^2 for the dynamic

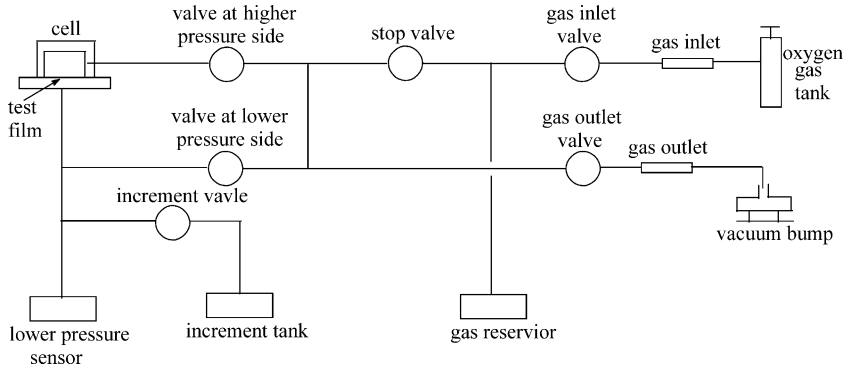

Fig. 2. Schematic of the experimental setup for measuring oxygen permeability of the film.

mechanical analysis (DMA). The storage modulus E', loss modulus E'', and loss tangent delta, tan δ, were determined in the temperature range between 30 and 130 °C using a dynamic mechanical analyzer (Perkin–Elmer DMA-7e). All measurements were carried out in a N_2 atmosphere at a frequency of 1 Hz and a heating rate of 5 °C/min. The melt-flow index (MFI) values of the nanocomposites were obtained using a Modular Flow Index machine (CEAST 6542/020) according to the specification, ASTM D 1238, at different temperatures. The rheological time tests were performed on a rheometer (Physica MC-200) with a parallel plate of 25 mm in diameter. A constant strain oscillatory shear mode was used for a small strain amplitude ($\gamma_0 = 1\%$) at 250 °C for 10 min to measure the complex viscosity of samples.

The mechanical properties of nanocomposites, including the tensile strength and Young's modulus and elongation at break (%), were determined in a tensile test. Rectangular-shape tensile test specimens of 1 mm in thickness were prepared by compression moulding according to the specification, ASTM D882. The tensile tests were performed at room temperature at a constant cross-head speed of 2.5 mm/min on a universal testing machine (Instron 5567).

The gas transmission rates of neat PETN and various PETN/clay nanocomposites were measured at room temperature using a gas permeability tester (K-315N, Rikaseiki, Japan). Fig. 2 shows the schematic of the experimental setup. The sample films were prepared by compression moulding of sheets of thickness approximately 150 μm, followed by melt-quenching using cold water. 100% pure oxygen was used for the test. The instrument consists of a cell separated into two parts by the membrane made of the sample film. Both parts of the cell were first subjected to vacuum to about 0.050 mm Hg. Oxygen was subsequently introduced into the upper part of the cell. The diffusion of oxygen across the sample film thickness took place due to the driving force resulting from the oxygen-pressure difference across it, and the gas contained in the lower part of the cell was analyzed using a pressure sensor. The gas permeability of films was characterized by the permeation coefficient, ρ (cc(stp) cm/cm^2·s·cm Hg):

$$\rho = \frac{L}{PAt} Q \tag{1}$$

where L is the film thickness (in cm), t is the time for permeation (in s), A is the area of gas transmission (in m^2) and Q is the gas transmission rate (in cc(stp)/m^2 h atm) measured by the instrument of film gas permeability tester. Q is given by:

$$Q = \frac{V}{A} \frac{273}{273 + \theta} \frac{1}{P} \frac{1}{\mathrm{d}t} \tag{2}$$

where V is the volume of the low pressure cell (in cm^3), θ is the temperature at the low pressure cell (in °C), P is the pressure difference between the two sides of the film before test (in mm Hg), and dt is the slope of the pressure vs. measuring time curve at a steady transmit state (in h).

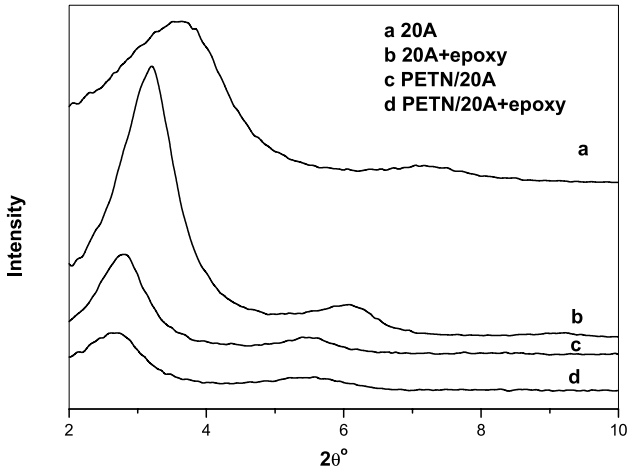

Fig. 3. XRD patterns of Cloisite 20A, epoxy premixed 20A and PETN/20A nanocomposites.

Table 1
Diffraction peak angle, 2θ, and the corresponding d-spacing d_{001} for organoclay and PETN/4 wt% clay nanocomposites

Sample	20A	30B	20A + epoxy	30B + epoxy
2θ (°)	3.65	4.85	3.2	2.8
d_{001} (nm)	2.42	1.82	2.83	3.15
Sample	PETN/20A	PETN/30B	PETN/20A + epoxy	PETN/30B + epoxy
2θ (°)	2.8	2.6	2.6	2.35
d_{001} (nm)	3.16	3.4	3.4	3.76

3. Results and discussion

3.1. Morphological structures of PETN/20A and PETN/30A systems

The morphology of the nanocomposites was studied using the XRD patterns and TEM observations The XRD patterns of as-received organoclays, organoclay premixed with epoxy and nanocomposites containing 4 wt% Cloisite 20A and 30B are presented in Figs. 3 and 4, respectively. The diffraction peak angles, 2θ, and the corresponding d-spacing d_{001}, obtained from these figures are summarized in Table 1. The primary silicate reflections at $2\theta = 3.65°$ for Cloisite 20A and at $2\theta = 5.1°$ for Cloisite 30B corresponded to d_{001} spacings of 2.42 and 1.73 nm, respectively. After premixing with epoxy, there were obvious shifts of the diffraction peak to lower angles, indicating intercalation of epoxy into the clay galleries. For the clay nanocomposites, a broad peak in the small-angle region indicates the formation of partially exfoliated/intercalated structures. However, the PETN/Cloisite 20A hybrid showed a larger number of organoclay agglomerates with an associated small increase in d-spacing from 2.42 to 3.16 nm, indicating a negligible improvement in intercalation. In contrast, a significant improvement in d_{001} spacing by 1.5 nm was noted for the PETN/Cloisite 30B composite, as compared to the pristine Cloisite 30B.

A rheological time test was performed to evaluate the effect of different clay modifiers on viscosity of PETN at melting temperatures. The time dependence of complex viscosity of the nanocomposites is presented in Fig. 5. For the PETN/30B system, the complex viscosity value was about 3 times that of the PETN/20A system. This result along with the above d-spacing values indicate that the interactions between the hydroxyl groups in the organic modifier of Cloisite 30B and the carbonyl end groups in PETN were more pronounced than those between the non-polar group of the modifier in Cloisite 20A and PETN molecules. Similar phenomena were also reported previously for a similar polyester/Cloisite30B system [34,35]. The incorporation of epoxy monomer into the PETN/clay nanocomposites improved the nanostructures of the corresponding hybrids, especially for the PETN/30B system. A further increase in d-spacing and a decrease in the intensity of diffraction peak were noted fro the XRD curves (Figs. 3(d) and 4(d)). An epoxy monomer was successfully added to the PBT/30B system [35] as the compatibilizer in melt processing to realize nanoscale dispersion, resulting in acceleration of intercalation of the PBT chains into the silicate galleries due to the miscibility between epoxy resin and PBT. In the present study, epoxy was intercalated between the silicate layers before melt-intercalation with PETN. Within the time constraint of extrusion operations, epoxide is a most suitable functionality to form covalent bonds with the nucleophilic end groups present in

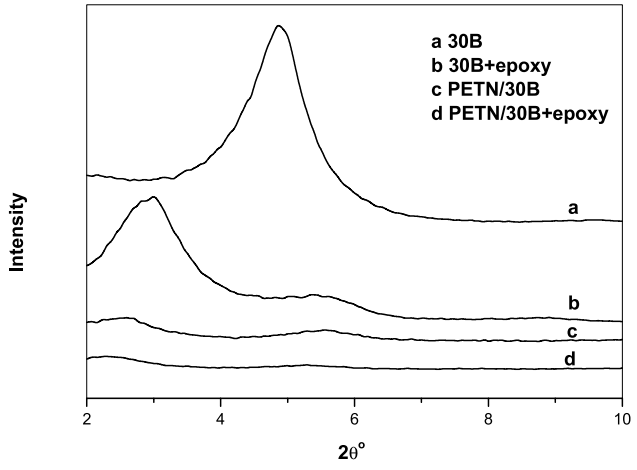

Fig. 4. XRD patterns of Cloisite 30B, epoxy premixed 30B and PETN/30B nanocomposites.

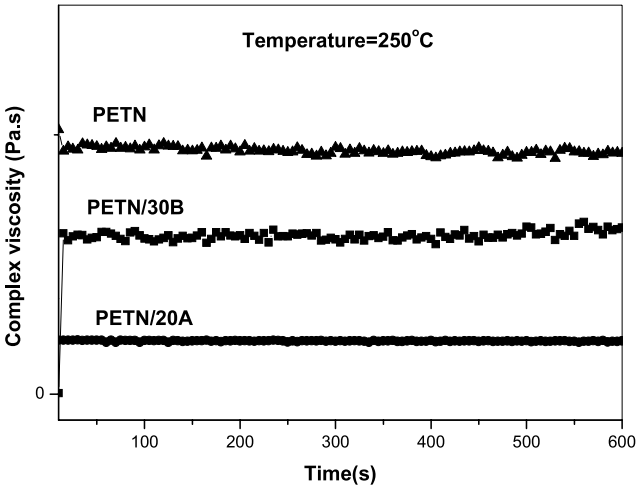

Fig. 5. Rheological time test curves for neat PETN, PETN/Cloisite 20A and PETN/Cloisite 30B nanocompoistes at 250 °C.

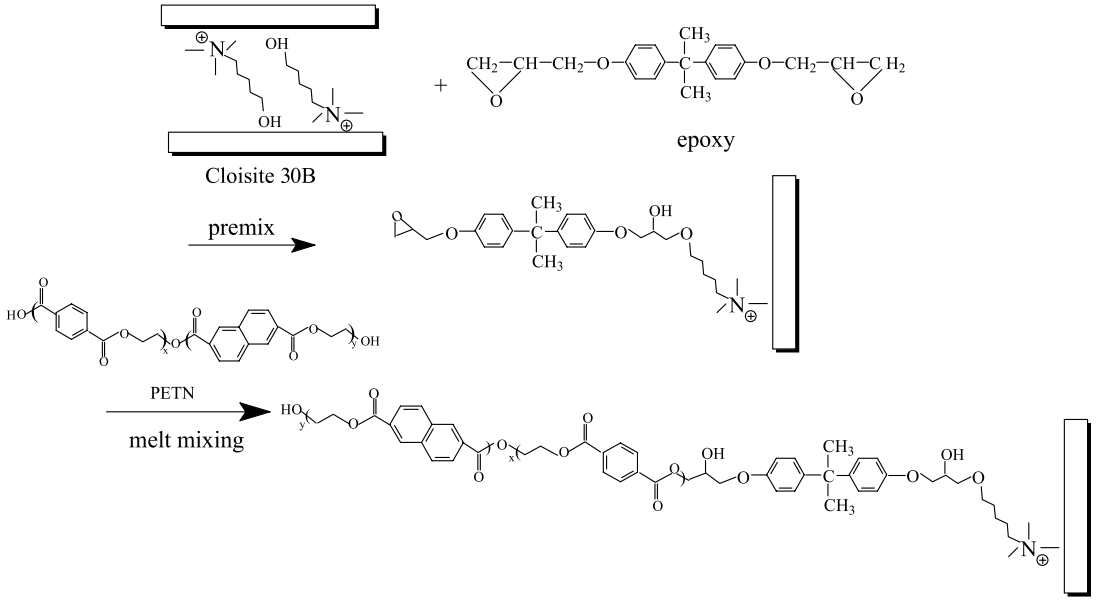

Fig. 6. Schematic presentation of intercalation of epoxy and PETN into Cloisite 30B interlayers.

polyesters. Such melt reactions between epoxide groups, hydroxyl groups in Cloisite 30B modifier and the carboxyl end groups of PETN were expected to take place, introducing extensive intercalation and exfoliation of Cloisite 30B. These reactions are schematically illustrated in Fig. 6, where epoxy acts as the compatibilizer as well as the chain extender. It is noted that the effect of epoxy on exfoliation in the PETN/20A system was not as significant as in the PETN/30B hybrid, a similar observation made previously [35]. The difference between Cloisites 20A and 30B comes from the ammonium cations located in the gallery of the silicate layers. With two bulky tallow groups, the ammonium cations present in Cloisite 20A are hydrophobic, while those in Cloisite 30B are more hydrophilic with their two hydroxyethyl groups. Due to the hydroxyl groups, the methyltallowbis (2-hydroxyethyl) ammonium cations in the Cloisite 30B interlayer allowed strong polar interactions with the carboxyl groups present in PETN, favoring the intercalation of PETN chains and the formation of PETN/Cloisite 30B nanocomposites. In contrast, strong polar interactions were lacking between the ammonium cations present in Cloisite 20A and the PETN chains, discouraging the PETN intercalation. In summary, Cloisite 30B is a more favorable choice for fabricating PETN/clay nanocomposite than Cloisite 20A, and a focused study was made on the PETN/30B system for the rest of this paper.

The partially exfoliated/intercalated structure in the PETN/30B system is further supported by TEM micrographs presented in Fig. 7. Partially exfoliated/intercalated, individual clay platelets and small stacks of intercalated montmorillonites are randomly distributed in the PETN matrix of the PETN/30B and PETN/30B/epoxy systems. The absence of large aggregates in both the systems further confirms the compatibility of Cloisite 30B organoclay with PETN. The more uniform dispersion and higher degree of intercalation/exfoliation of epoxy-treated Cloisite 30B than the virgin Cloisite 30B also partly confirmed the chemical interactions illustrated in Fig. 6.

3.2. Thermomechanical and flow properties

Fig. 8 shows the DSC cooling and second heating curves of neat PETN and PETN/30B composites obtained at a constant ramp rate of 10 °C/min. The thermal parameters obtained from these curves, including melting point, T_m, crystallization temperature, T_c, and the enthalpy of crystallization, ΔH_c, are summarized in Table 2. The DSC thermogram (Fig. 8(b)) indicates that the melting endotherms of the PETN/30B hybrids were virtually unchanged from that of the neat PETN regardless of clay content and the epoxy treatment. This observation may suggest that the well-developed thick lamellae in the PETN matrix remain largely unchanged even after incorporation of organoclay. It is interesting to note that the incorporation of organoclay into PETN resulted in a large increase in crystalline temperature, T_c, and normalized crystallization heat, ΔH_c (Fig. 8(a)). This behavior was expected and is associated with the strong heterogeneous nucleation effect

Table 2
Thermal transition parameters of neat PETN and PETN/4 wt% cloisite 30B nanocomposites measured by DSC

Sample	T_c (°C)	T_m (°C)	ΔH_c (J/g)
Neat PETN	161.4	240.1	10.24
PETN/30B	177.7	239.6	42.53
PETN/30B/epoxy	171.3	239.5	40.05

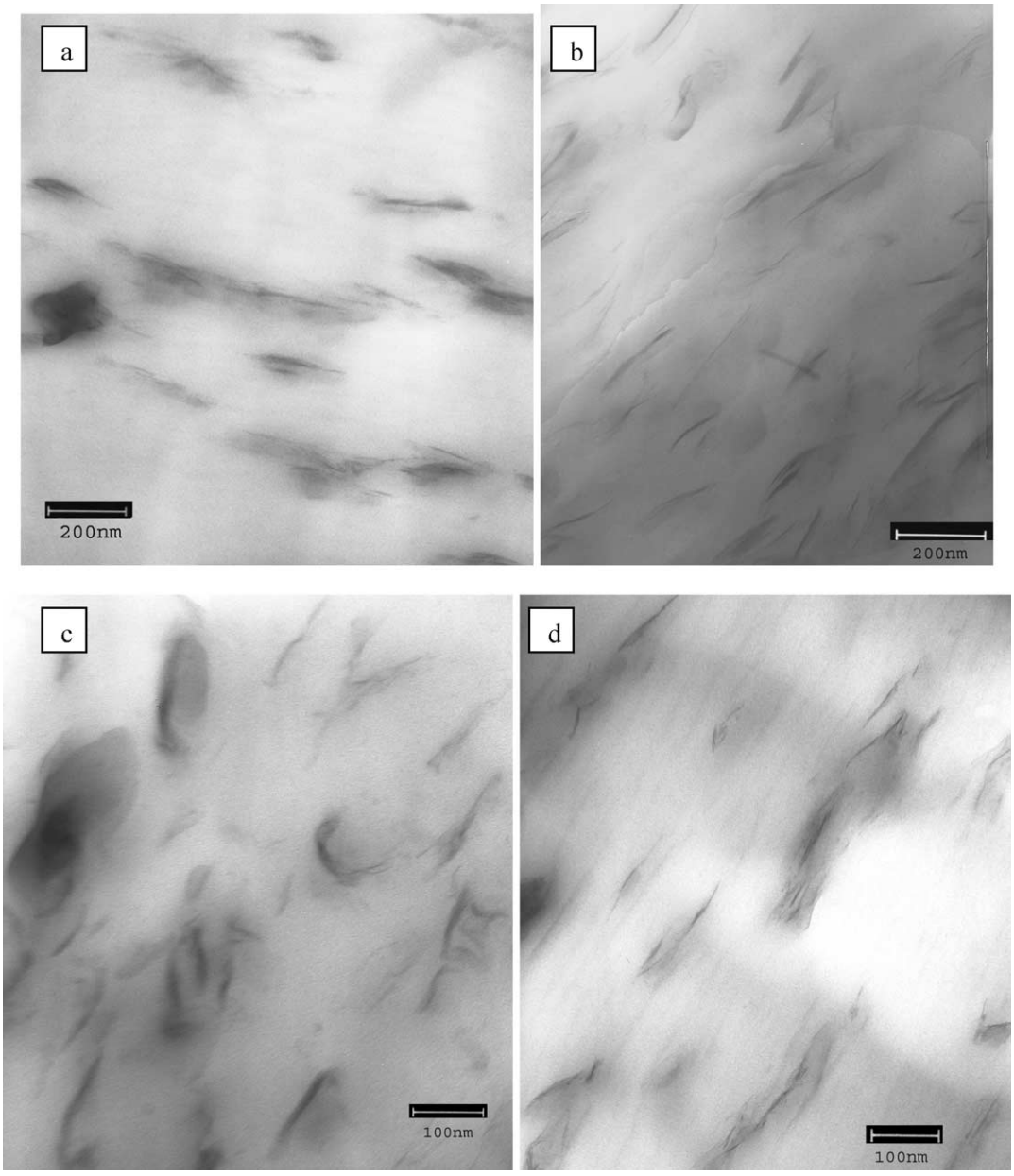

Fig. 7. TEM micrographs of (a), (c) PETN/Cloisite 30B and (b), (d) PETN/Cloisite 30B/epoxy hybrid at different magnifications.

of the clay particles [22,24]. On the other hand, the PETN/30B/epoxy system presented a lower T_c than the PETN/30B composite, implying slower crystallization rate, which is attributed to the epoxy acting as the compatibilizer and chain extender between the clay and PETN matrix. The longer PETN molecular chains and the stronger interactions between the clay and PETN stemming from the epoxy treatment restricted the movements of chain segments and hindered the folding of molecular chains into lamella, thus decelerating the rate of crystallization.

Storage modulus, E', and loss modulus, E'', of neat PETN and PETN/30B nanocomposites were obtained from the dynamic mechanical analysis (Fig. 9). The storage modulus was higher in the order of PETN/30B/epoxy hybrid, PETN/30B composite and neat PETN over the entire temperature range studied. The higher storage modulus for the composite treated with epoxy than that without reflects the higher mechanical stability of the former composite. The glass transition temperatures, T_g, determined from the values corresponding to the loss modulus peaks exhibited basically the same trend although the differences between the different materials were marginal. A similar observation was reported for the PETN/expandable fluorine mica nanocomposites compatibilized by 10-[3,5-bis(methoxycarbonyl) phenoxy]decyltriphenylphosphonium bromide (IP10TP) [36]. The reason was ascribed to an improved

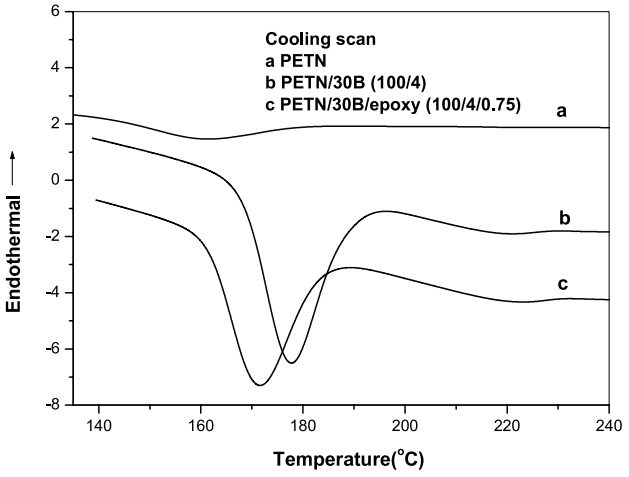

(a)

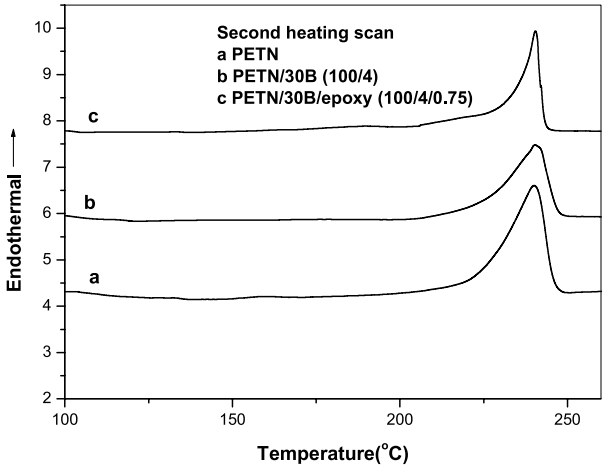

(b)

Fig. 8. Endotherms of PETN and PETN/Cloisite 30B hybrids measured by DSC during (a) cooling and (b) the second heating at a constant rate of 10 °C/min.

interaction between the PETN and clay due to the bromide and the constraint of PETN chain segment movements by the exfoliated silicates in the composite.

In polymer matrix composites, the mechanical response reflects molecular relaxation characteristics of the matrix, but is also profoundly influenced by external factors arising, for example, from the constraint of chain movement near the rigid filler surface [37]. The increase in storage modulus and T_g due to clay particles could be attributed to the hindrance of macromolecular mobility of polymer chains caused by the well-dispersed Cloisite 30B silicate layers in the PETN matrix, as proven in other thermoplastic polymer/clay systems [34,38]. The more pronounced enhancement of mechanical properties arising from the small amount of epoxy addition was due both to the improved interaction between the organoclay Cloisite 30B and PETN by the epoxy compatibilizer and the chain extension effect of epoxy in the PETN matrix discussed in the following section.

The thermal stability of PETN and PETN/30B composites were investigated by TGA and the original and derivatives of the thermogravimetric curves are presented in Fig. 10. The peak values of derivative curves corresponding to the decomposition temperatures, T_d, are included in the figure. The composite with 4 wt% Cloisite 30B possessed higher thermal stability by 3 °C than the neat PETN, while epoxy treatment of clay surface brought about a remarkable 17.4 °C increase in T_d. The improvement in thermal stability is a direct reflection of excellent thermal barrier effect of layered clay within the matrix [22,23,39]. The much higher T_d of the PETN/30B/epoxy system suggests that the epoxy acted as strong chain extender between the clay and PETN matrix. Thermal degradation mechanisms of PET during melt processing involved random alkyl-oxygen chain scission. Acetaldehyde, water, carbon dioxide and carboxyl end groups are the main products of thermal degradation of PET [40].

Not only was the increase in decomposition temperature, but also a consistent viscosity at wider temperature range for melt intercalation of PETN/30B nanocomposite was realized by the epoxy treatment of organoclay. The melt flow index (MFI) vs. temperature is plotted for the neat PETN, PETN/30B and PETN/30B/epoxy systems in Fig. 11. MFI is the output flow rate (in gram) of a polymer, which occurs in 10 min through a standard die of 2.0955 mm in diameter and 8.0 mm in length when a constant pressure is applied to a melt via a piston. A high MFI is related to a low melt strength, which in turn reflects a poor processability during extrusion. The melt strength of PETN cannot be measured if its MFI is above 200 [41]. Poly(ethylene terephthalate) (PET) is relatively difficult to process compared to other thermoplastics, such polystyrene, polyethylene, polypropylene or polyvinyl chloride, because of PET's low melting viscosity when PET is processed via extrusion or injection molding. Chain extension has been extensively used to process resins with a low melt viscosity and melt strength. One of the attractive ways of improving melt strength of PET is to use the reactive chain extenders or modifiers such as multifunctional epoxy or anhydride compounds [41,42]. In this study, the MFI of the PETN/30B system increased rapidly with temperature and exceeded 210 at 255 °C; meanwhile the PETN/30B/epoxy system showed MFI values consistently lower than 100 and their melts could be extruded in the temperature range between 245 and 265 °C, the so-called 'process window', only 5 °C narrower than that of neat PETN. It was observed that the PETN/30B mixture could not be extruded at temperatures above 255 °C because of the low pressure at die and the low viscosity of the melt. Epoxies have been identified as one of the most suitable functionalities to

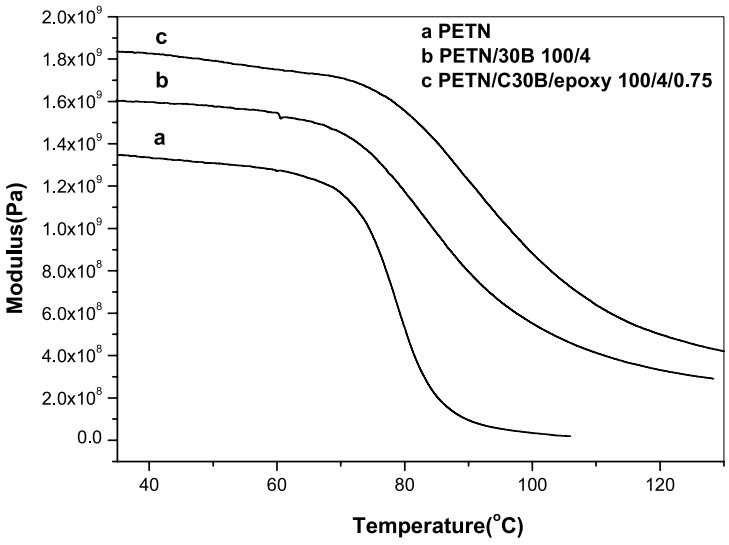

(a)

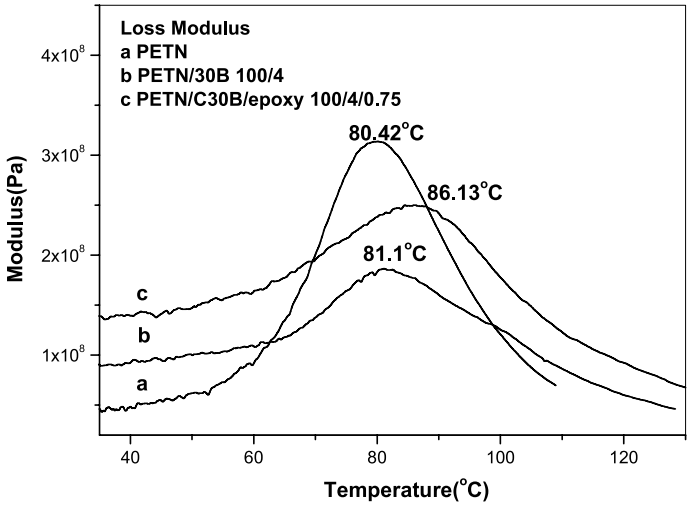

(b)

Fig. 9. Temperature dependence of (a) storage modulus (E') and loss modulus (E'') for neat PETN and PETN/4 wt% Cloisite 30B nanocomposites.

interact with the nucleophilic end groups (viz. hydroxyl and carboxyl) of PET within the residence time limits of extruder reactor. After the epoxy treatment, the melt viscosity increased significantly so that a steady flow was achieved even at a temperature as high as 265 °C. In other words, the epoxy treatment of organoclay gave rise to a widened processing window for melt intercalation of the nanocomposites.

3.3. Mechanical properties

The variation of tensile properties of PETN/30B nanocomposites with organoclay contents are shown in Fig. 12. The PETN/30B nanocomposites presented a higher tensile strength and modulus with increasing clay content, at the expense of reduced ductility. Filler particles are known to reduce the molecular mobility of polymer chains, producing a less flexible material with a higher tensile strength and Young's modulus [43]. With further increase in organoclay content beyond 4 wt%, the tensile strength of hybrids became a plateau value or even decreased. This observation suggests that there is an optimal amount of organoclay needed to achieve balanced property improvements, while avoiding agglomeration of clay particles [23,43,44]. The neat PETN was very ductile with an elongation at break over 150%, and increasing the clay content was

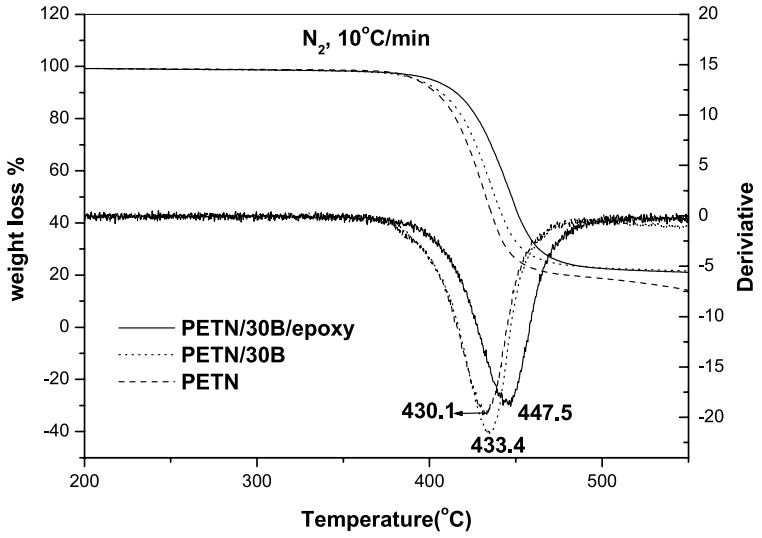

Fig. 10. Weight changes as a function of temperature for neat PETN and PETN/4 wt% Cloisite 30B nanocomposites.

detrimental to ductility. The large reduction in ductility especially at a high clay loading may also be associated with the unexfoliated clay particles, which acted as stress raisers in the matrix and caused premature failure.

Typical load–displacement curves of the PETN/30B nanocomposites with and without epoxy are shown in Fig. 13. The mechanical responses of the nanocomposite with organoclays treated with epoxy, were better than those of the PETN/30B composite at the same clay content. In particular, over 40% recovery in ductility was the achieved by treating the clay with epoxy. The PETN/30B composite exhibited a brittle fracture behavior, while the PETN/30B/epoxy system presented typical yielding curves indicating plastic deformation during loading. These observations suggest that the epoxy intercalated into the galleries and present on the surface of organoclays may have acted as a stress-relieving compliant medium, delaying the crack propagation along the interface between the clay and PETN matrix.

3.4. Gas permeability characteristics

Amorphous films of PETN and PETN/30B nanocomposites of the final film thickness of about 150 μm were prepared by melt moulding followed by quenching Fig. 14 presents typical O_2 gas transmission curves for neat PETN and PETN/30B nanocomposites. The permeation coefficients were calculated from the slopes of the steady state portion of the curves according to Eqs. (1) and (2), and are plotted in Fig. 15. The PETN/2 wt% 30B nanocomposite showed a remarkable 50% reduction in O_2 permeability, compared to the neat PETN. This observation is ascribed to

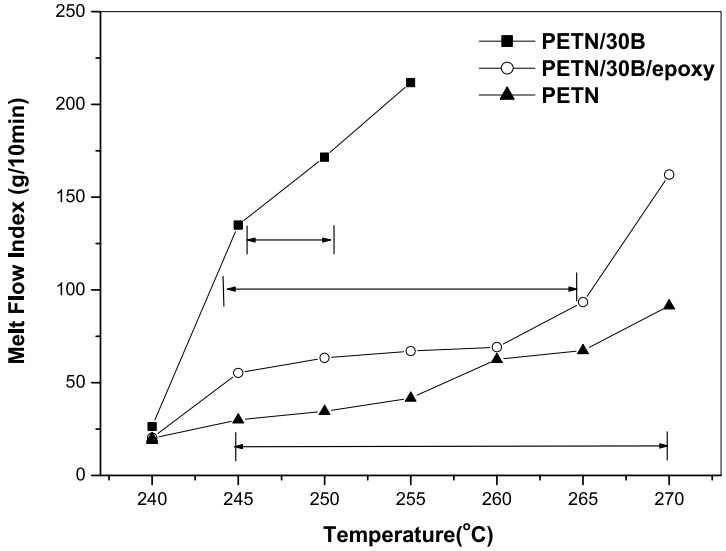

Fig. 11. Melt flow index as a function of temperature for PETN/Cloisite 30B and PETN/Cloisite 30B/epoxy nanocomposites. The arrows indicate the process windows.

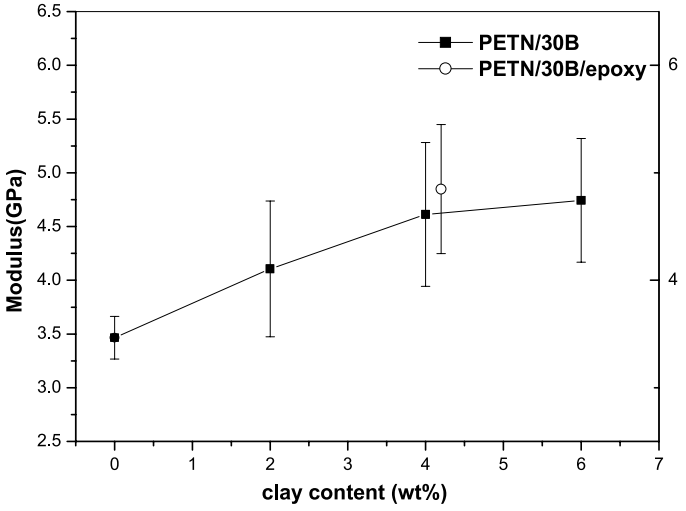

(a)

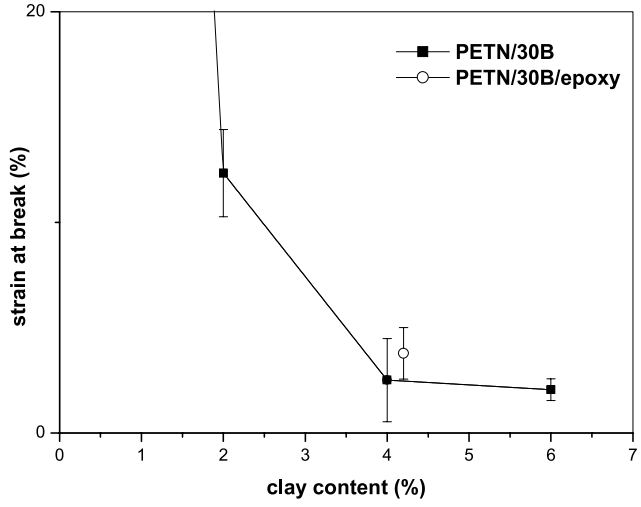

(b)

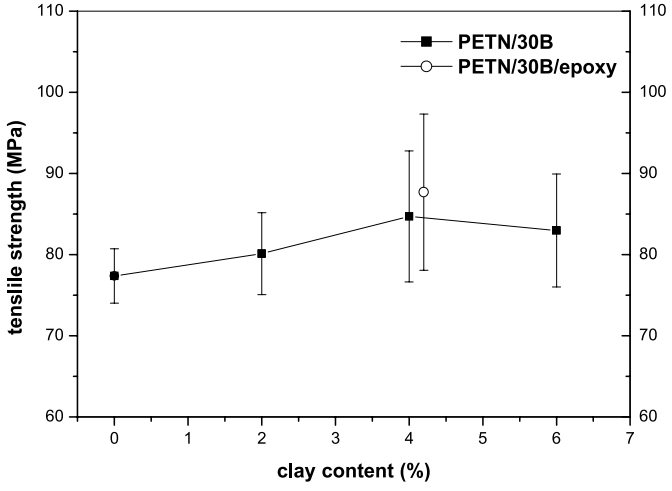

(c)

Fig. 12. (a) Tensile modulus, (b) strain at break and (c) tensile strength of PETN/Cloisite 30B nanocomposites as a function of clay content.

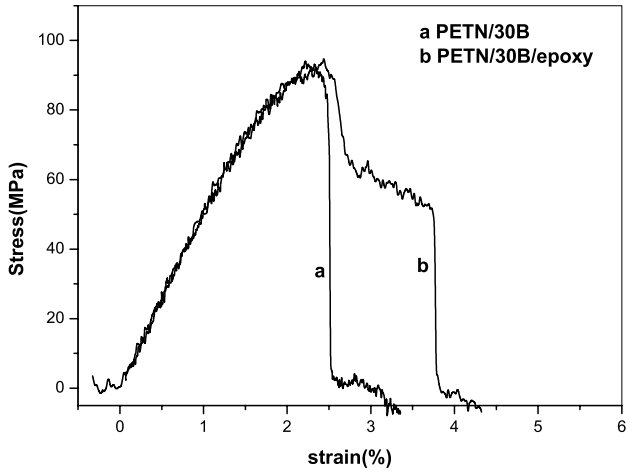

Fig. 13. Tensile stress–strain curves for (a) PETN/4 wt% 30B and (b) PETN/4 wt% 30B/epoxy nanocomposites.

the tortuous path for diffusing gas molecules, which were created by the nano-scale silicate layers with a huge aspect ratio (in the range of 300–600). Further increase in clay loading above 4 wt% did not improve systematically the gas permeation resistance. However, with the addition of epoxy, a more than 88% reduction in gas permeability compared to the neat PETN was achieved. This result suggests that the uniform dispersion of organoclay particles and the improved interactions along the organoclay–PETN matrix interface benefited from the epoxy treatment also played an important role in improving the gas barrier characteristics of PETN/clay nanocomposites.

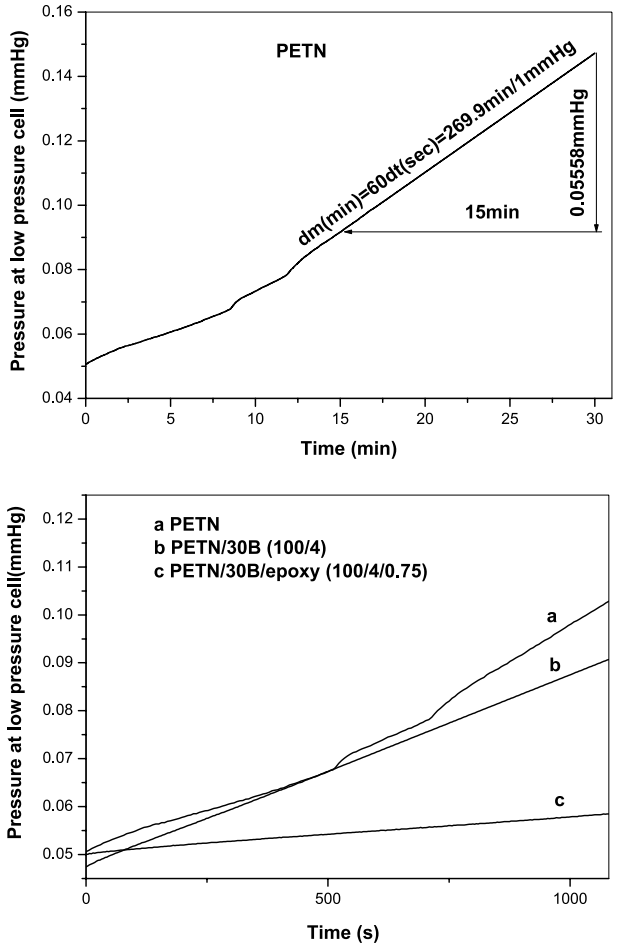

Fig. 14. Plots of oxygen transmission rate for neat PETN and PETN/30B nanocomposites.

4. Conclusions

The morphological, thermo-mechanical, rheological, tensile and gas barrier properties were studied of PETN nanocomposites containing two different organoclays, Cloisite 20A and 30B. The following can be highlighted from the study.

(i) Although the inherent *d*-spacing between the silicate layers of Cloisite 30A was narrower than Cloisite 20A (1.73 vs. 2.42 nm), the PETN/30B system exhibited more significant increase in *d*-spacing than the PETN/20A system (with the final *d*-spacing of 3.15 vs. 2.83 nm) after melt mixing with PETN. Treatment of the organoclays with epoxy monomer before mixing with PETN further improved the intercalation/exfoliation, especially of the PETN/30B system, suggesting that the epoxy acted as the compatibilizer as well as the chain extender.

(ii) The addition of Cloisite 30B organoclays into PETN resulted in an increase in crystalline temperature, T_c, and normalized crystallization heat, ΔH_c, as well as in storage and loss moduli and glass transition temperature. Treatment of organoclay further increased these properties, except T_c. All these changes in thermo-mechanical properties reflect the hindrance of macromolecular mobility of polymer chains caused by the well-dispersed silicate layers within the matrix.

(iii) The epoxy treatment of clay surface resulted in a remarkable 17.4 °C increase in decomposition temperature as measured from TGA, reflecting the ameliorating effect on thermal stability of the composites. The epoxy treatment also resulted in a significant improvement in melt flow index of the PETN/30B/epoxy system even at a high temperature, giving rise to a much wider process window of 245–265 °C than 245–250 °C for the PETN/30B.

(iv) The organoclay reinforcement gave rise to a higher tensile strength and modulus than the neat PETN, at the expense of much reduced ductility. Epoxy treatment of organoclay resulted in further, albeit marginal, improvements of all three tensile properties, partly confirming the improved interactions between functional groups in epoxy, PETN matrix and organoclay surface.

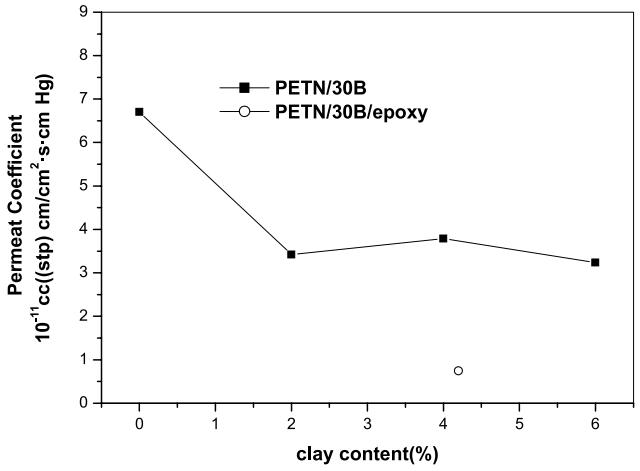

Fig. 15. Permeation coefficient as a function of clay content for PETN/30B nanocomposites.

(v) The gas permeability of PETN film decreased by 50% with the addition of 2 wt% 30B organoclay, followed by little changes with further increase in clay content. Epoxy treatment of organoclay further improved the gas barrier characteristics of the PETN/30B nanocomposites, suggesting the importance of uniform dispersion and chemical interactions of organoclay particles in improving the gas barrier characteristics of nanocomposites.

Acknowledgements

This project was supported by the Research Grant Council of Hong Kong and ML was a visiting scholar from the Changchun Institute of Applied Chemistry, Chinese Academy of Sciences to HKUST on a PDF Matching Fund Scheme when this work was done. Most experiments were carried out with technical supports from the Materials Characterization and Preparation Facilities (MCPF) and Advanced Engineering Materials Facilities (AEMF). The gas permeation test was performed with the assistant of Prof Benzhong Tang of Chemistry Department of HKUST.

References

[1] Kiersnowski A, Piglowski J. Polymer-layered silicate nanocomposites based on poly(ε-caprolactone). Eur Polym J 2004;40:1199–207.
[2] Park CI, Choi WM, Kim MH, Park OO. Thermal and mechanical properties of syndiotactic polystyrene/organoclay nanocomposites with different microstructures. J Polym Sci, Part B: Polym Phys 2004; 42:1685–93.
[3] Fornes TD, Hunter DL, Paul DR. Effect of sodium montmorillonite source on nylon 6/clay nanocomposites. Polymer 2004;45:2321–31.
[4] Gopakumar TG, Lee JA, Kontopoulou M, Parent JS. Influence of clay exfoliation on the physical properties of montmorillonite/polyethylene composites. Polymer 2002;43:5483–91.
[5] Jin BK, Wu XS, Chen DZ, He PS. Elastomeric stamp made by the silicon rubber modified with montmorillonite. Chem J Chin Univ (Chinese) 2003;24:1142–4.
[6] Huang JC, Zhu ZK, Yin J, Qian X, Sun YY. Poly(etherimide)/montmorillonite nanocomposites prepared by melt intercalation: morphology, solvent resistance properties and thermal properties. Polymer 2001;42:873–7.
[7] Yeh JM, Liou SJ, Chang YW. Polyacrylamide–clay nanocomposite materials prepared by photopolymerization with acrylamide as an intercalating agent. J Appl Polym Sci 2004;91:3489–96.
[8] Maiti P, Yamada K, Okamoto M, Ueda K, Okamoto K. New polylactide/layered silicate nanocomposites: role of organoclays. Chem Mater 2002;14:4654–61.
[9] Kim JK, Hu CG, Woo RSC, Sham ML. Moisture barrier characteristics of organoclay–epoxy nanocomposites. Compos Sci Technol 2005;14:805–13.
[10] Hu CG, Kim JK. Epoxy-organoclay nanocomposites: morphology, moisture absorption behavior and thermo-mechanical properties, Compos Interf 2005, in press.
[11] Qin HL, Su QS, Zhang SM, Zhao B, Yang MS. Thermal stability and flammability of polyamide 66/montmorillonite nanocomposltes. Polymer 2003;44:7533–8.
[12] Liu YL, Hsu CY, Wei WL, Jeng RJ. Preparation and thermal properties of epoxy–silica nanocomposites from nanoscale colloidal silica. Polymer 2003;44:5159–67.
[13] Jimenez G, Ogata N, Kawai H, Ogihara T. Structure and thermal/mechanical properties of poly(1-caprolactone)-clay blend. J Appl Polym Sci 1997;64:2211–20.
[14] Ogata N, Jimenez G, Kawai H, Ogihara T. Structure and thermal/mechanical properties of poly(L-lactide)–clay blend. J Polym Sci, Part B: Polym Phys 1997;35:389–96.
[15] Greenland DJ. Adsorption of poly(vinyl alcohols) by montmorillonite. J Colloid Sci 1963;18:647–64.
[16] Usuki A, Kawasumi M, Kojima Y, Okada A, Kurauchi T, Kamigaito O. Swelling behavior of montmorillonite cation exchanged for ω-amine acid by ε-caprolactam. J Mater Res 1993;8:1174–8.
[17] Wang Z, Pinnavaia T. Nanolayer reinforcement of elastomeric polyurethane. Chem Mater 1998;10:3769–71.
[18] Pantoustier N, Alexandre M, Degee P, Calberg C, Jerome R, Henrist C, et al. Poly(ε-caprolactone) layered silicate nanocomposites: effect of clay surface modifiers on the melt intercalation process. e-Polymer 2001;9:1–9.
[19] Ray SS, Okamoto M. Polymer/layered silicate nanocomposites: a review from preparation to processing. Prog Polym Sci 2003;28: 1539–641.
[20] Cho JW, Paul DR. Nylon 6 nanocomposites by melt compounding. Polymer 2001;42:1083–90.
[21] Defosse MT. PETN enjoys explosive demand, rising prices. Mod Plast 2000;77:53–4.
[22] Ou CF, Ho MT, Lin JR. Synthesis and characterization of poly(ethylene terephthalate) nanocomposites with organoclay. J Appl Polym Sci 2004;91:140–5.
[23] Chang JH, Park DK. Various organo-clays based nanocomposites of poly(ethylene terephthalate-*co*-ethylene naphthalate). Polym Bull 2001;47:191–7.
[24] Ke YC, Long CF, Qi ZN. Crystallization, properties, and crystal and nanoscale morphology of PETN–clay nanocomposites. J Appl Polym Sci 1999;71(7):1139–46.
[25] Ke YC, Yang ZB, Zhu CF. Investigation of properties, nanostructure, and distribution in controlled polyester polymerization with layered silicate. J Appl Polym Sci 2002;85(13):2677–91.
[26] Chang JH, Kim SJ, Joo YL, Im S. Poly(ethylene terephthalate) nanocomposites by in situ interlayer polymerization: the thermomechanical properties and morphology of the hybrid fibers. Polymer 2004;45:919–26.
[27] Zhang GZ, Shichi T, Takagi K. PETN–clay hybrids with improved tensile strength. Mater Lett 2003;57:1858–62.

[28] Imai Y, Nishimura S, Abe E, Tateyama H, Abiko A, Yamaguchi A, et al. High-modules poly(ethylene terephthalate)/expandable fluorine mica nanocomposites with a novel reactive compatibilizer. Chem Mater 2002;14:477–9.
[29] Sanchez-Solis A, Garcia-Rejon A, Manero O. Production of nanocomposites of PETN-montmorillonite clay by an extrusion process. Macromol Symp 2001;92:281–92.
[30] Pegoretti A, Kolarik J, Peroni C, Migliaresi C. Recycled poly (ethylene terephthalate)/layered silicate nanocomposites: morphology and tensile mechanical properties. Polymer 2004;45:2751–9.
[31] Davis CH, Mathias LJ, Gilman JW. Effects of melt-processing conditions on the quality of poly(ethylene terephthalate) montmorillonite clay nanocomposites. J Polym Sci, Part B: Polym Phys 2002; 40:2661–6.
[32] Matayabas JC, Turner SR, Sublett BJ, Connell GW, Barbee RB. PCT Int Appl WO, 98/29499 (Eastman Chemical Co.); 1998.
[33] Bikiaris DN, Karayannidis GP. Effect of carboxylic end groups on thermooxidative stability of PETN and PBT. Polym Degrad Stab 1999;63:213–8.
[34] Di YW, Iannace S, Di ME, Nicolais L. Nanocomposites by melt intercalation based on polycaprolactone and organoclay. J Polym Sci, Part B: Polym Phys 2003;41:670–8.
[35] Li XC, Kang TY, Cho WJ, Lee JK, Ha CS. Preparation and characterization of poly(butyleneterephthalate)/organoclay nanocomposites. Macromol Rapid Commun 2001;22:1306–12.
[36] Saujanya C, Imai Y, Tateyama H. Structure and thermal properties of compatibilized PETN/expandable fluorine mica nanocomposites. Polym Bull 2002;49:69–76.
[37] Paul DR, Newman S. Polymer blends. New York: Academic Press; 1978. p. 353–4.
[38] Riva A, Zanetti M, Braglia M, Camino G, Falqui L. Thermal degradation and rheological behaviour of EVA/montmorillonite nanocomposites. Polym Degrad Stab 2002;77:299–304.
[39] Zhu ZK, Yang Y, Yin J, Wang XY, Ke YC, Qi ZN. Preparation and properties of organosoluble montmorillonite polyimide hybrid materials. J Appl Polym Sci 1999;73:2063–8.
[40] Pohl HA. The thermal degradation of polyesters. J Am Chem Soc 1951;73:5660–1.
[41] Xanthos M, Wan C, Dhavalikar R, Karayannidis GP, Bikiaris DN. Identification of rheological and structural characteristics of foamable poly(ethylene terephthalate) by reactive extrusion. Polym Int 2004;53: 1161–8.
[42] Xanthos M, Dey SK. In: Lee ST, editor. Principles of thermoplastic foam extrusion. Lancaster, PA: Technomic Publishing Co; 2000. p. 307–36.
[43] Gu AJ, Kuo SW, Chang FC. Syntheses and properties of PI/clay hybrids. J Appl Polym Sci 2001;79:1902–10.
[44] Yang Y, Zhu ZK, Yin J, Wang XY, Qi ZN. Preparation and properties of hybrids of organo-soluble polyimide and montmorillonite with various chemical surface modification methods. Polymer 1999;40: 4407–14.